[4] Cappozzo, A. et al., 1996, ''Position and Orientation in Space of Bones During Movement: Experimental Artefacts,'' Clin. Biomech. (Los Angel. Calif.), **11**(2), pp. 90–100.
[5] Korvick, D. L., Pijanowski, G. J., and Schaeffer, D. J., 1994, ''Three-Dimensional Kinematics of the Intact and Cranial Cruciate Ligament-Deficient Stifle of Dogs,'' J. Biomech., **27**(1), pp. 77–87.
[6] Tashman, S., and Anderst, W., 2003, ''In-Vivo Measurement of Dynamic Joint Motion Using High Speed Biplane Radiography and CT: Application to Canine ACL Deficiency,'' J. Biomech. Eng., **125**(2), pp. 238–245.
[7] Lafortune, M. A. et al., 1992, ''Three-Dimensional Kinematics of the Human Knee During Walking,'' J. Biomech., **25**(4), pp. 347–357.
[8] Reinschmidt, C. et al., 1997, ''Tibiocalcaneal Motion During Running, Measured With External and Bone Markers,'' Clin. Biomech. (Los Angel. Calif.), **12**(1), pp. 8–16.
[9] Ramsey, D. K., and Wretenberg, P. F., 1999, ''Biomechanics of the Knee: Methodological Considerations in the in Vivo Kinematic Analysis of the Tibiofemoral and Patellofemoral Joint,'' Clin. Biomech. (Los Angel. Calif.), **14**(9), pp. 595–611.
[10] Ramsey, D. K. et al., 2001, ''Assessment of Functional Knee Bracing: An in Vivo Three-Dimensional Kinematic Analysis of the Anterior Cruciate Deficient Knee,'' Clin. Biomech. (Los Angel. Calif.), **16**, pp. 61–70.
[11] Stacoff, A. et al., 2001, ''Effects of Shoe Sole Construction on Skeletal Motion During Running,'' Med. Sci. Sports Exercise, **33**(2), pp. 311–319.
[12] Woltring, H. J., 1986, ''A FORTRAN Package for Generalized Cross-Validatory Spline Smoothing and Differentiation,'' Advances in Engineering, **8**, pp. 104–113.
[13] Soderkvist, I., and Wedin, P. A., 1993, ''Determining the Movements of the Skeleton Using Well-Configured Markers,'' J. Biomech., **26**(12), pp. 1473–1477.
[14] Grood, E. S., and Suntay, W. J., 1983, ''A Joint Coordinate System for the Clinical Description of Three-Dimensional Motions: Application to the Knee,'' J. Biomech. Eng., **105**(2), pp. 136–144.
[15] American Society for Testing and Materials, 2002, ''Standard Practice for Use of the Terms Precision and Bias in ASTM Test Methods, Vol. 14.02,'' Annual Book of ASTM Standards, E177.
[16] Ramakrishnan, H. K., and Kadaba, M. P., 1991, ''On the Estimation of Joint Kinematics During Gait,'' J. Biomech., **24**(10), pp. 969–977.

Electrical Impedance Tomography of Cell Viability in Tissue With Application to Cryosurgery

Rafael Davalos*
e-mail: rvdaval@sandia.gov

Boris Rubinsky
e-mail: rubinksy@me.berkeley.edu

Biomedical Engineering Laboratory—Department of Mechanical Engineering, 6178 Etcheverry Hall—University of California at Berkeley, Berkeley CA, 94720-1740

Tissue damage that is associated with the loss of cell membrane integrity should alter the bulk electrical properties of the tissue. This study shows that electrical impedance tomography (EIT) should be able to detect and image necrotic tissue inside the body due to the permeabilization of the membrane to ions. Cryosurgery, a minimally invasive surgical procedure that uses freezing to destroy undesirable tissue, was used to investigate the hypothesis. Experimental results with liver tissue demonstrate that cell damage during freezing results in substantial changes in tissue electrical properties. Two-dimensional EIT simulations of liver cryosurgery, which employ the experimental data, demonstrate the feasibility of this application. [DOI: 10.1115/1.1695577]

*Corresponding author.
Contributed by the Bioengineering Division for Publication in the JOURNAL OF BIOMECHANICAL ENGINEERING. Manuscript received by the Bioengineering Division March 27, 2003; revision received July 15, 2003. Associate Editor: C. Dong.

Introduction

In many medical applications, it is important to distinguish between live and dead cells in vivo. For instance, after cancer treatments, mechanical injury, or exposure to hypothermia or hypoxia, it is essential to know whether the targeted or traumatized cells are alive or not. Methods for measuring brain activity, to assess tissue viability after a stroke, are being made available [1,2]. However, with the exception of brain tissue assessment, there is currently no method to determine cell viability in vivo and, therefore, no process to quantify the success of certain surgical procedures or the severity of an accident. In this research we show that cell viability in tissue can be determined through measurement of cell electrical impedance. We also show that electrical impedance tomography (EIT) can be used as a tool for viability detection.

There are two ways to determine cell viability: through their function or through their properties. Viability can be tested through cell function by, for example, measuring metabolism, the ability to process glucose, with positron emission tomography (PET). One of the most common methods for determining viability through cell properties is by assessing the integrity of the cell membrane, a primary distinguishing feature separating live cells from dead cells. When membrane integrity is lost, chemicals that would otherwise not enter the cell can now enter. Therefore, membrane integrity tests for cells in suspension [3] and cells in excised tissue [4] have been designed to test for the presence of chemicals inside cells that normally cannot penetrate the membranes of viable cells. The use of normally impermeant dyes that fluoresce once inside the cell, such as YOYO-1 (Molecular Probes OR) [5], is common in these tests.

In this study, we propose another method for detecting membrane integrity of cells inside tissue, derived from the use of fluorescent dyes for viability detection. The cell membrane, in addition to preventing macromolecules from entering the cell, also functions as an ionic-transport barrier, preventing low-frequency current from entering the cell. Therefore, when the membrane is compromised, ions as well as fluorescent dyes can pass through the cell. Consequently, cell necrosis as indicated by cell membrane damage should lead to a measurable decrease in electrical resistivity of the bulk tissue. The intent of this research is to show that in tissue, cell membrane integrity can be determined by measuring this change using a bioimpedance technique.

Electrical properties of cells and tissues have been the subject of much research during the last century. Electrical tissue data is available and has been tabulated in many books and review articles [6–9]. Tissue is an inhomogeneous material with intracellular and extracellular conductive domains and is strongly characterized by the presence of the cell membrane, which has high capacitance and a low but complex conductance [9]. Experiments have shown that the electrical properties of tissue are, therefore, highly dependent on frequency. Of particular importance to this study is the observation that the permittivity of tissue decreases in three major steps, termed alpha, beta and gamma, and is roughly constant between these steps [9]. The steps roughly occur in the frequency range of milli-Hz to Hz, kHz to 100 MHz and 0.1 to 100 GHz, respectively [6,9]. The alpha dispersion in the Hz range is related to membrane molecular phenomena such as counterion effects, gated channels and intercellular structures. The gamma dispersion in the GHz range is related to dipolar mechanisms in the polar water, salts and proteins. Of particular interest for this study is the beta dielectric dispersion, which is due to the buildup of charges at the cell membrane and interfacial or Maxwell-Wagner type of polarization [9]. Therefore in this study, to determine the integrity of the cell membrane after cryosurgery, we employed kHz frequency.

Electrical impedance tomography is a bioimpedance technique that relies on the differences in bioelectrical attributes between tissues to produce an image representing the spatial tissue impedance distribution inside the body or organ. Electrodes surround the body and a sub-sensory current pattern is injected into the body

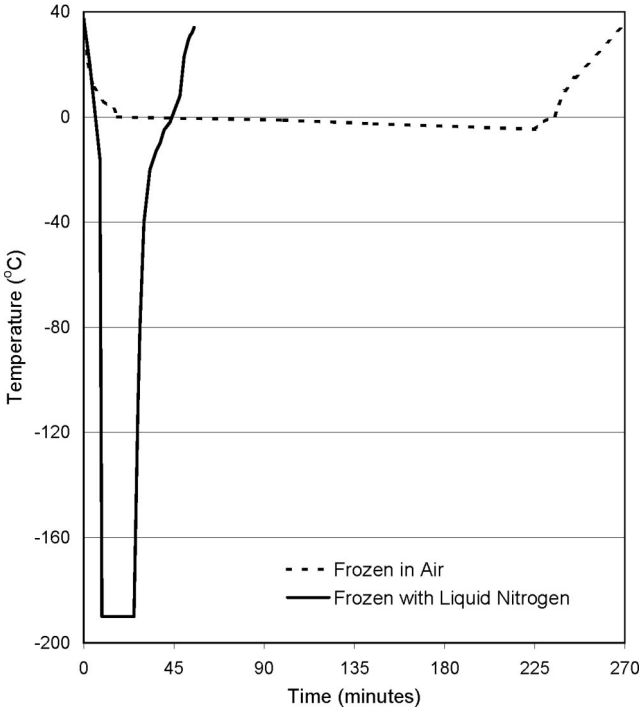

Fig. 1 Thermal history of liver tissue frozen in air and frozen using liquid nitrogen.

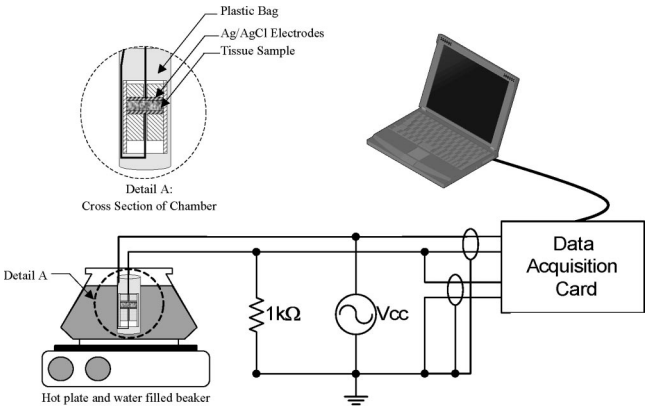

Fig. 2 Schematic of experimental setup.

through electrode pairs while the ensuing potentials are measured on the remaining electrodes. A reconstruction algorithm uses these voltage measurements, the current pair information, and electrode geometries to produce an image. Reconstruction algorithms generally use a pixel-based approach where the imaging region is divided into a number of impedance pixels. Algorithms find a solution iteratively, employing a numerical method, since the inverse solution to the Poisson equation is usually nonlinear. After an initial guess of the impedance distribution, usually uniform, the impedance of each pixel is adjusted until the system converges on some solution to an objective function, resulting in an image. For a general overview of EIT, see [10]. Since EIT produces an image representing the spatial tissue impedance distribution inside the body or organ we, therefore, propose that the change in tissue electrical resistivity upon the loss of cell membrane integrity could be imaged with EIT.

This paper investigates whether electrical properties could be used in situations in which it is vital to distinguish between living and dead tissue using cryosurgery as a specific application. Cryosurgery is a surgical procedure that destroys tissue by freezing it with a cryogen cooled surgical probe that is in contact with the targeted tissue [11,12]. With the advent of imaging techniques to monitor in real-time the extent of the frozen lesion, imaging monitored cryosurgery is now often used in the treatment of prostate and liver cancer [11,12]. However, it was found that indiscriminant freezing does not necessarily destroy tissue [3,4,13,14]. Instead, tissue destruction is a function of the thermal parameters applied during freezing. For example, in a complimentary study with rat liver ex vivo, it has been shown that antifreeze proteins could serve as an adjuvant to cryosurgery. Even though the percentage of tissue destruction along the outer margin of the cryolesion, the most likely area for survival and regression, was increased, the results were vastly dependent on the thermal protocols, in this case thermal cycles, applied [4]. Therefore, while the extent of freezing can be exquisitely monitored with an array of imaging techniques, the effective application of cryosurgery is still hampered by that fact that the extent of freezing does not necessarily correspond to the extent of tissue destruction. Because there is no imaging method to evaluate the effectiveness of a procedure, research continues. In what may become an important application of this study, we first compare experimentally between the electrical characteristics of tissue frozen with thermal conditions that ensure damage and tissue with thermal conditions in which cells survive. Then the experimental data is incorporated into an EIT model to determine if the changes in electrical resistivity between tissue destroyed by freezing and tissue that survives freezing can be used to develop an EIT image of tissue treated by cryosurgery.

Methods

Preparation of Liver Tissue. An experimental procedure was carried out to evaluate the changes in electrical properties of tissue following freezing with thermal parameters that cause tissue destruction and with thermal parameters in which the tissue survives freezing. The experiments were performed with fresh liver tissue from Spraque-Dawley rats, excised within minutes after the animals were anesthetized. After excision, the rat liver was sectioned in 2 mm thick slices and frozen either in liquid nitrogen or in air at $-20°C$ and then rapidly thawed in a saline solution at $37°C$.

Thermal Protocols. The electrical resistivity of rat liver was measured for three scenarios: following excision; after it was frozen using liquid nitrogen ($-190°C$); and after it was slowly frozen in air at $-20°C$. Figure 1 shows the thermal history for the last two cases, as measured by thermocouples inserted in the tissue. The tissue frozen using liquid nitrogen reached a minimum of $-190°C$ while the tissue frozen in air reached a minimum of $-4.7°C$. In cryosurgery, the frozen tissue experiences a wide range of cooling rates and freezing temperatures. Studying the electrical properties of frozen tissue in the entire range of combinations of cooling rates and temperature is beyond the scope of this preliminary study. In this paper we roughly focused on only two combinations typical to the inner and outer limits of the frozen lesion. The first is near the probe, where freezing occurs rapidly to liquid nitrogen temperatures, and the second is on the outer edge of the lesion, where freezing occurs slowly to high subzero temperatures. These particular thermal parameters were chosen because they produce either complete tissue destruction by freezing (liquid nitrogen) or greater than 90% frozen hepatocyte survival ($-20°C$ air) [4]. Liver tissue was chosen because it is relatively homogenous and, therefore, relatively macroscopically isotropic, which eliminates any issues with the orientation of the electrodes with respect to the tissue. Five tissue samples were measured within a 10-minute span for each of the four sets of experimental conditions. All electrical measurements were re-

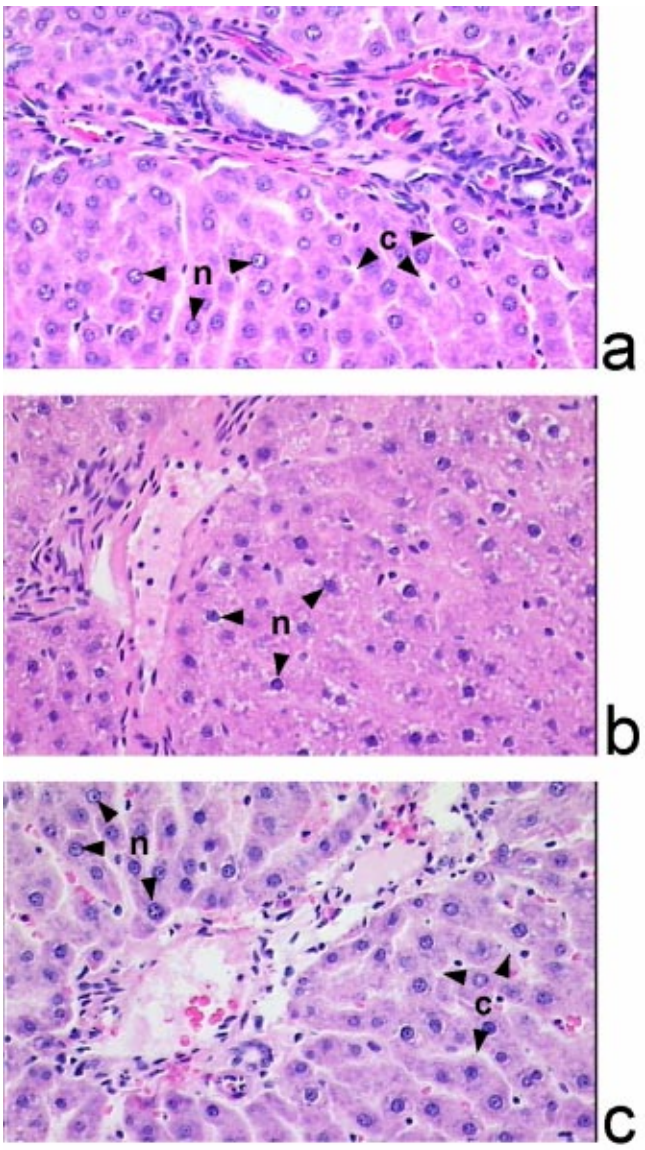

Fig. 3 Histological samples of rat liver at 200× magnification, showing the nuclei (n) and cytoplasmic limits (c) *a*: freshly excised sample *b*: sample frozen with liquid nitrogen *c*: sample frozen in air.

corded for 30 seconds and conducted at body temperature (37°C). The freshly excised measurements were taken within an hour of excision while measurements for the tissue treated with liquid nitrogen and for the tissue frozen in air were taken approximately 55 and 270 minutes thereafter, respectively, as depicted in Fig. 1. The tissue was stored in 0.9% aqueous solution until use.

Electrical Impedance Measurements. Resistivity measurements were conducted by placing excised tissue into a nonconductive chamber with a 2.0 cm^2 circular cross-section between two 12 mm diameter electrodes (In vivo Metric, Healdsburg, CA). Figure 2 is a schematic of the experimental setup. To minimize contact resistance, silver/silver chloride electrodes with large surface areas were used with a sinusoidal input. A 1 kHz current was injected from one electrode through the sample and out the other electrode. The amount of current through the tissue was determined by measuring the voltage drop across a 1 kOhm resistor located between the last electrode and ground.

The sinusoidal waveform is generated from a function generator and converted using a dual-op-amp (JFET TLO82CP) voltage-to-current converter (VCC), which is powered by a Raytheon (864107-4) 25V power supply. The system is controlled with a National Instruments PCI-1200 data acquisition card and coded using National Instruments LabVIEW 6.1 acquisition software (National Instruments, Austin, TX).

Histology. To investigate the structural integrity of the tissue following each of the three scenarios, the samples were prepared using a hematoxylin and eosin stain and mounted on a microscope slide (PSI Berkeley, CA). Figure 3*a* shows a histological section of the freshly excised tissue at 200×. It shows excellent preservation of the hepatocytes and the absence of cytoplasmic lysis. The limits between cytoplasms as well as the sinusoids are clearly visible. It also shows that the inner structures of the nuclei were well preserved.

Figure 3*b* shows the histological section of the tissue that was cooled using liquid nitrogen with a subsequent thaw and indicates that the tissue was severely damaged by the treatment. At 200× magnification, it shows that the vascular structures are recognizable but the cytoplasmic limits of the hepatocytes have all but disappeared. The sinusoids and endothelial cells are not visible, and lysis of the cytoplasm is very intense. It also shows that most of the nuclei and the inner structure were not visible.

Figure 3*c* shows a histological section of the tissue that was frozen in air to −4.7°C with a subsequent thaw. At 200× magnification, it can be seen that some of the cytoplasms exhibited an early lysis and that some of the sinusoids are not clearly visible. However, the morphology is similar, in general, to that of the fresh sample and the nuclei were well preserved.

Numerical Methods. As a first step towards demonstrating feasibility of electrical impedance tomography for tissue viability detection, we created 2-D simulations representing liver tissue, containing one or more small sections of damaged tissue. We incorporated the electrical measurements from the experiments into the models for the electrical properties of the tissue and attempted to produce an image of this simulated phantom using a standard reconstruction algorithm.

For each simulation, 32 electrodes were equally spaced around the model periphery. A 1-mA current was injected through opposite electrode pairs (''projections'') while recording the voltage differences across the remaining opposite pairs (known as an ''opposite-opposite'' data collection algorithm [15]). For each current projection, the resulting voltages were obtained by solving the Poisson equation in a finely meshed finite-element system, using the resistivity distribution from the simulated phantom. We assumed that the liver is temporarily placed in an electrically insulating, semi-rigid electrode array fixture during the surgical procedure. Therefore, a zero flux boundary condition was imposed along the periphery of the simulation except at the locations of the source and sink electrodes, and electrode placement uncertainty errors were not considered.

The collection of ensuing voltage measurements produces a vector of independent voltage measurements whose vector length defines the maximum number of independent variables (in our case, 464 impedance pixels) for a well-defined matrix inverse to exist. An image was then produced from the known current inputs, the electrode geometry, and the measured voltage data using the reconstruction algorithm.

We employed a modified Newton-Raphson (NR) reconstruction algorithm because of its excellent convergence properties [16]. The method attempts to iteratively minimize an objective function representing the difference between the overall voltage measurements from the simulated phantom and the measurements from the reconstruction algorithm's internal model. The Jacobian matrix was calculated using a sensitivity matrix approach [17] employing Marquardt regularization to overcome the ill-conditioning [18].

The internal model to the reconstruction algorithm contained a finite element mesh with an inner imaging region of 366 triangular

Table 1 Resistivity change of rat liver at 37°C exposed to two freezing conditions

		mean±std [Ω cm]	*p* *t*-test
Freezing with liquid nitrogen (n=5)	Prior to treatment	2038±140	
	After treatment	739±43	0.00004
Freezing with air (n=5)	Prior to treatment	2011±184	
	After treatment	2234±128	0.14333

elements and an outer ring with a constrained constant resistivity. For these parameters, the convergence criteria for this algorithm were typically met after approximately 20 iterations, taking approximately 5 minutes.

Numerical models were solved using MATLAB's partial differential equation toolbox (The MathWorks Inc., Natick, MA). Data acquisition and computations were conducted on a Compaq 1700 Presario laptop computer with an Intel 800-MHz processor and 256MB of RAM.

Results

The experiments indicated that the resistivity of the liver would drop from a normalized value of 1(0.068) to 0.363(0.026) for the samples cooled with liquid nitrogen and change from 0.987(0.090) to 1.096(0.063) for the samples frozen in air. The number in parenthesis is the normalized standard deviation from a sample size of five. The results have been normalized using 2038 Ω cm, the mean value of the freshly excised tissue measurements prior to liquid nitrogen freezing, and a summary of the results can be found in Table 1. It is evident that the liver frozen with thermal conditions that do not induce damage retained its electrical properties, while liver frozen under conditions that induce cell necrosis experienced a statistically significant (*t*-test: $p \ll 1$) decrease in electrical resistivity. These results agree with the histology assessment, which shows little distinction between the freshly excised tissue and the tissue frozen in air but tremendous difference between the freshly excised tissue and the tissue frozen using liquid nitrogen. The results also confirm the hypothesis that cell membrane damage causes a decrease in the bulk tissue electrical resistivity because the cell membrane no longer inhibits ionic current.

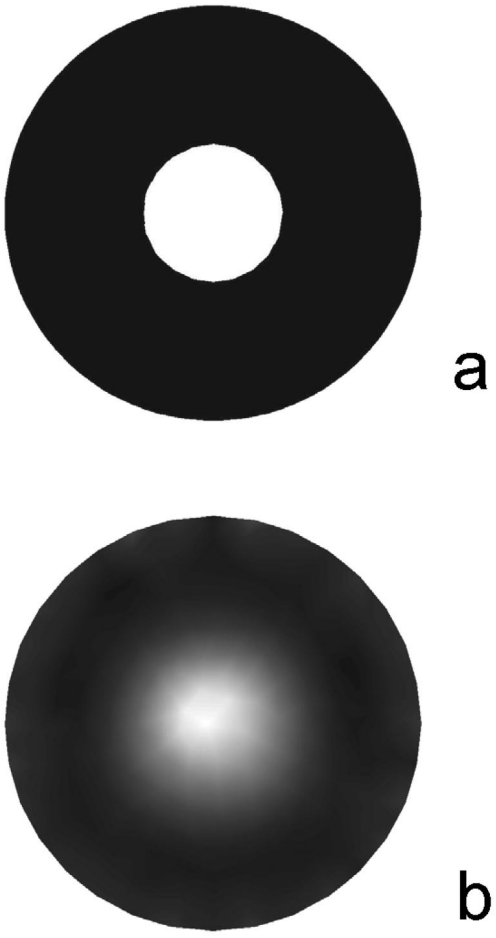

Fig. 4 First post-cryosurgical configuration: 6 cm imaging domain ($1.0\rho_o$) with a 2 cm circular damaged region ($0.363\rho_o$) located in the center of the domain *a*: Simulated phantom *b*: Generated image.

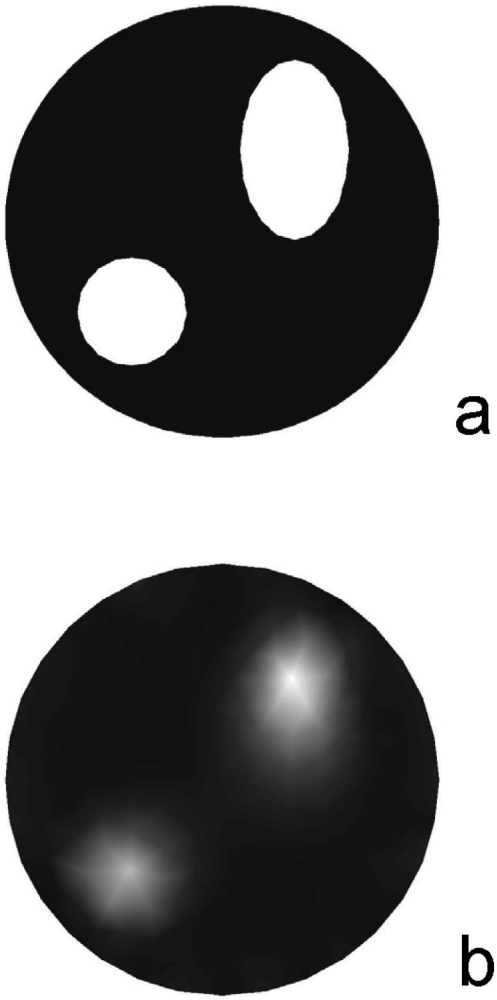

Fig. 5 Second post-cryosurgical configuration: 6 cm imaging domain ($1.0\rho_o$) with a 1.5 cm×2.5 elliptical section and a 1.5 cm circular section that are damaged ($0.363\rho_o$) *a*: Simulated phantom *b*: Generated image.

Two different resistivity maps were generated as examples of two different distributions of damaged tissue inside an undamaged imaging region, 6 cm in diameter. The simulations incorporated the resistivity values from the cryosurgery experimental results, $1.0\rho_o$ Ω cm (from the freshly excised tissue measurements prior to liquid nitrogen freezing) for the healthy tissue and $0.363\rho_o$ Ω cm (from the tissue frozen with liquid nitrogen measurements) for the damaged tissue.

Figures 4*a* and 4*b* show the simulated phantom and generated image, respectively, for the first scenario. In this example, the damaged tissue is circular, 2 cm in diameter, located in the center of the undamaged tissue. The second scenario has two damaged

regions inside the tissue, an elliptical region, 1.5 cm×2.0 cm, located towards the upper right with a circular region, 1.5 cm in diameter, located in the lower left area of the tissue. Figures 5*a* and 5*b* show the resistivity map and generated image for the second example, respectively. In both examples, the reconstruction algorithm accurately generated an image representing the size and location of the damaged tissue, which indicates that EIT could be used to image tissue damaged by cryosurgery.

Conclusion

This study investigated whether electrical measurements could be used in situations in which it is vital to distinguish between healthy and damaged tissue in vivo using a specific application, cryosurgery. Cell membrane integrity is one of the most commonly used methods to detect cell viability for ex vivo and in vitro applications. Because the loss of integrity of the cell membrane also changes the bulk bioelectrical properties of the tissue, EIT may provide an inexpensive and flexible supplement to imaging techniques for assessing membrane integrity in vivo. From our simulated phantoms, which incorporated the experimental data, we successfully generated 2-D EIT images representing the spatial distribution of the tissue damaged by cryosurgery. Complexities that have to be addressed at later stages include: real world inhomogeneities from larger blood vessels, patient-to-patient variations, the effect of noise on image quality, nonplanar currents in 3-D regions, and nonlinear electrode behaviors. Many of these issues should be resolvable through further reconstruction algorithm refinements and a more rigorous set of experiments. Nevertheless, the results in this study suggest that EIT may eventually be able to image damaged tissue following a cryosurgical procedure and, potentially, viability of tissue in general for other in vivo applications.

Acknowledgments

This research was supported by NIH grant 5RO1 RR14591. Rafael Davalos would like to acknowledge Sandia National Laboratories for general support of his research. Sandia is a multiprogram laboratory operated by Sandia Corporation, a Lockheed-Martin company, for the United States Department of Energy under contract DE-AC04094AL85000.

References

[1] Vokow, N. D., Ding, Y.-S., Fowler, J. S., and Gatley, S. J., 2001, ''Imaging Brain Cholinergic Activity with Positron Emission Tomography: Its Role in the Evaluation of Cholinergic Treatments in Alzheimer's Dementia,'' Society of Biological Psychiatry, **49**, pp. 211–220.
[2] Preece, M., Mukherjee, B., Huang, C. L.-H., Hall, L. D., Leslie, R. A. and, and James, M. F., 2001, ''Detection of Pharmacologically Mediated Changes in Cerebral Activity by Functional Magnetic Resonance Imaging: The effects of sulpiride in the brain of the anaesthetised rat,'' Brain Res., **916**, pp. 107–114.
[3] Rui, J., Tatsutani, K. N., Dahiya, R., and Rubinsky, B., 1999, ''Effect of Thermal Variables on Human Breast Cancer in Cryosurgery,'' Alcohol Drug Res., **53**(2), pp. 185–192.
[4] Koushafar, H., Pham, L., Lee, C., and Rubinsky, B., 1997, ''Chemical Adjuvant Cryosurgery with Antifreeze Proteins,'' J. Surg. Oncol., **66**, pp. 114–121.
[5] Haugland, R. P., 1996, Handbook of Fluorescent Probes and Research Chemicals: Molecular Probes, Inc.
[6] Schwan, H. P., 1957, ''Electrical Properties of Tissue and Cell Suspensions.'' Adv. Biol. Med. Phys., **5**, pp. 147–209.
[7] Schwan, H. P., and Kay, C. F., 1957, ''The conductivity of living tissue.'' Ann. NY Acad. Sci., **65**, pp. 1007–1013.
[8] Stuchly, M. A., and Stuchly, S. S., 1990, ''Electrical Properties of Biological Substances'' in *Biological effects and medical applications of electromagnetic energy*, O. P. Gandhi, Ed., Prentice Hall, Englewood City, NJ.
[9] Grimnes, S., and Martinsen, Ø. G., 2000, *Bioimpedance and Bioelectricity Basics*, Academic Press, New York, NY.
[10] Boone, K., Barber, D., and Brown, B., 1997, ''Review–Imaging with Electricity: Report of the European Concerted Action on Impedance Tomography,'' J. Med. Eng. Technol., **21**(6), pp. 201–232.
[11] Rubinsky, B., 2000, ''Cryosurgery,'' in *Annual Reviews in Biomedical Engineering*, vol. 2, M. L. Yarmish, K. R. Diller, and M. Toner, Eds., Annual Review Press, Palo Alto, CA, pp. 157–187.
[12] Rubinsky, B., 2002, ''Low Temperature Preservation of Biological Organs and Tissues,'' in Future Strategies for Tissue and Organ Replacement, J. M. Polak, L. L. Hench, and P. Kemp, Eds. Imperial College Press, London, UK, pp. 27–49.
[13] Tatsutani, K. N., and Rubinsky, B., 1998, ''A Method to Study Intracellular Nucleation,'' ASME J. Biomech. Eng., **120**(1), pp. 27–31.
[14] Pham, L., and Rubinsky, B., 1998, ''Breast Tissue Cryosurgery with Antifreeze Proteins,'' Adv. heat and mass transfer in biotechnology, **40**, pp. 171–175.
[15] Rigau, B., and Morucci, J. P., 1996, ''Bioelectrical Impedance Techniques in Medicine: Part III: Impedance Imaging: First Section: General Concepts and Hardware,'' Crit. Rev. Biomed. Eng., **24**(4–6), pp. 467–597.
[16] Yorkey, T. J., and Webster, J. G., 1987, ''A Comparison of Impedance Tomographic Reconstruction Algorithms,'' Clin. Phys. Physiol. Meas., **8**(11), pp. 55–62.
[17] Gencer, N. G., Ider, Y. Z., and Williamson, S. J., 1996, ''Electrical Impedance Tomography: Induced-current Imaging Achieved with a Multiple Coil System,'' IEEE Trans. Biomed. Eng., **43**(2), pp. 139–149.
[18] Marquardt, D. W., 1963, ''An Algorithm for Least-squares Estimation of Nonlinear Parameters,'' J. Appl. Mech., **11**, pp. 431–441.

Measurements of Mouse Pulmonary Artery Biomechanics

Naomi C. Chesler*
Department of Biomedical Engineering, University of Wisconsin, Madison, WI and Department of Mechanical Engineering, University of Vermont, Burlington, VT

John Thompson-Figueroa and Ken Millburne
Department of Internal Medicine, University of Vermont, Burlington, VT

Background: *Robust techniques for characterizing the biomechanical properties of mouse pulmonary arteries will permit exciting gene-level hypotheses regarding pulmonary vascular disease to be tested in genetically engineered animals. In this paper, we present the first measurements of the biomechanical properties of mouse pulmonary arteries.*
Method of Approach: *In an isolated vessel perfusion system, transmural pressure, internal diameter and wall thickness were measured during inflation and deflation of mouse pulmonary arteries over low (5–40 mmHg) and high (10–120 mmHg) pressure ranges representing physiological pressures in the pulmonary and systemic circulations, respectively.*
Results: *During inflation, circumferential stress versus strain showed the nonlinear "J"-shape typical of arteries. Hudetz's incremental elastic modulus ranged from $27\pm13\,kPa$ $(n=7)$ during low-pressure inflation to $2{,}700\pm1{,}700\,kPa$ $(n=9)$ during high-pressure inflation. The low and high-pressure testing protocols yielded quantitatively indistinguishable stress-strain and modulus-strain results. Histology performed to assess the state of the tissue after mechanical testing showed intact medial and adventitial architecture with some loss of endothelium, suggesting that smooth muscle cell contractile strength could also be measured with these techniques.*
Conclusions: *The measurement techniques described demonstrate the feasibility of quantifying mouse pulmonary artery biomechanical properties. Stress-strain behavior and incremental modulus values are presented for normal, healthy arteries over a wide pressure range. These techniques will be useful for investigations into biomechanical abnormalities in pulmonary vascular disease.*
[DOI: 10.1115/1.1695578]

*Corresponding author: Department of Biomedical Engineering, University of Wisconsin-Madison, 2146 Engineering Centers Building, 1550 Engineering Drive, Madison, WI 53706-1609. Phone: 608 265-8920; Fax: 608 265-9239; e-mail: Chesler@engr.wisc.edu.

Contributed by the Bioengineering Division for publication in the JOURNAL OF BIOMECHANICAL ENGINEERING. Manuscript received by the Bioengineering Division May 27, 2003; revision received September 23, 2003. Associate Editor: M. S. Sacks.